(PVDF)$_2$(PEO)$_2$ miktoarm star copolymers: Synthesis and isothermal crystallization leading to exclusive β-phase formation

Nicolás María [a], Yogesh Patil [b], George Polymeropoulos [b], Anatoly Peshkov [b], Valentin Rodionov [b], Jon Maiz [a,c,d,*], Nikos Hadjichristidis [b,*], Alejandro J. Müller [a,c,*]

[a] POLYMAT and Department of Polymers and Advanced Materials: Physics, Chemistry and Technology, University of the Basque Country UPV/EHU, Paseo Manuel de Lardizabal 3, 20018 Donostia-San Sebastián, Spain
[b] Polymer Synthesis Laboratory, KAUST Catalysis Center, Physical Sciences and Engineering Division, King Abdullah University of Science and Technology (KAUST), Thuwal 23955-6900, Kingdom of Saudi Arabia
[c] IKERBASQUE, Basque Foundation for Science, Plaza Euskadi 5, 48009 Bilbao, Spain
[d] Centro de Física de Materiales (CFM) (CSIC–UPV/EHU) – Materials Physics Center (MPC), Paseo Manuel de Lardizabal 5, 20018 San Sebastián, Spain

ARTICLE INFO

ABSTRACT

In this work, we study how chain topology can induce different polymorphic behaviors in poly(vinylidene fluoride) (PVDF)-based materials. A linear PVDF precursor with two azido groups at the junction point, (PVDF$_x$-N$_3$)$_2$ and three 4-miktoarm star copolymers (PVDF$_x$)$_2$-b-(PEO$_y$)$_2$ with two poly(ethylene oxide) (PEO) and two PVDF arms were synthesized and employed in this study. The amphiphilic miktoarm copolymers were prepared by a combination of anionic ring-opening polymerization, iodine transfer radical polymerization (ITP), and copper-catalyzed azide-alkyne cycloaddition (CuAAC). They have practically similar overall molar mass but different compositions, ideal for performing bulk morphology and crystallization investigations. The isothermal overall crystallization kinetics of the PVDF and PEO arms of the 4-miktoarm star copolymers and representative PEO and PVDF precursors was determined by Differential Scanning Calorimetry (DSC). The results indicate that the star arms crystallized faster than the equivalent precursors as the kinetics are dominated by nucleation effects. The phases formed by the PVDF components in the materials examined were analyzed by studying their melting behavior by DSC, their superstructural morphology by Polarized Light Optical Microscopy (PLOM), and the phase structure by Fourier Transform Infrared Spectroscopy (FTIR). The linear PVDF and (PVDF$_{29}$-N$_3$)$_2$, exhibited α, β and γ-phases (with a majority of β-phase formation) during melting after isothermal crystallization. The ratio of the different phases depends on the crystallization temperature. An analysis of the multiple melting behavior indicated that the sample forms both α and β-phases initially, and the α-phase partially transforms into the γ-phase during isothermal crystallization when the temperature of crystallization increases. We found a remarkable behavior for the 4-miktoarm star copolymers, as the PVDF arms only form the ferroelectric β-phase when all three materials were isothermally crystallized regardless of the crystallization temperature employed. The presence of the polymorphism in the PVDF was detected by DSC, PLOM, and FTIR. Hence, we have shown that tailoring chain topology in PVDF copolymers can lead to exclusive β-phase formation, a path that can be exploited for future piezoelectric applications.

1. Introduction

Research in new materials focused on improving renewable energy yields to avoid carbon emissions is increasing to keep the environment safe. Clean energy sources like those derived from specific materials combined with natural mechanical efforts to convert them into harvested energy have to be developed in the following years. During the last decades, inorganic materials have been used for these purposes, but in recent years polymers are replacing them in view of their advantageous properties, such as low density, flexibility, efficiency, and low cost [1].

In this context, fluoropolymers, especially poly(vinylidene fluoride)

(PVDF), have been extensively investigated both in academia and industry because of their exceptional properties and remarkable applications [2]. PVDF is an exciting material thanks to its ferroelectric and piezoelectric properties [3–5],and mechanical properties [6]. These properties make this material a valuable tool in various applications, such as data storage, energy harvesting, or sensors, as long as the ferroelectric and piezoelectric properties are present [7]. One of the limitations of PVDF is that the desired crystalline phase is not always obtained as the material is polymorphic. The relationship between processing-structure–function has to be studied to find the best crystallization conditions that result in the most favorable polymorphic phases [8]. PVDF has four well-known crystalline phases, i.e., α, β, γ, and δ [9]. Still, not all of them are polar phases, which are the most interesting ones to achieve the optimum ferroelectric and piezoelectric properties. Another novel application of PVDF is the functionalization of carbon nanotubes through different polymerization processes [10].

The most pursued and desired crystalline phase in PVDF for electrical applications is the β-phase due to its polarization magnitude [11]. The β-phase is characterized by a high dipole moment perpendicular to the chain axis. Of the four crystalline PVDF phases, the β-phase has the highest piezoelectric effect. The crystalline structure of the β-phase is made of chains with all fluorides in a *trans* position ($TTTT$) [12], which help its polarization. However, when a linear PVDF is crystallized from the melt at typical cooling rates (20 °C/min), a paraelectric crystalline α-phase is obtained [13]. This paraelectric crystalline phase is the most commonly encountered and stable in PVDF. The chains are in a *trans-gauche* conformation ($TG^+TG^-TG^+TG^-$) in the α-phase crystals [14]. For the above-mentioned purposes, and the construction of electronic devices, the crystalline α-phase is not appropriate.

There are two other minor polar crystalline phases [15,16]. One of them is the γ-phase, characterized by a $TTTG^+TTTG^-$ chain conformation in the crystal and by displaying ferroelectric properties [16]. The second one, the so-called δ-phase is similar to the α-phase, as they share the same crystal lattice parameters and chain conformation (TG^+TG^-). But there are also differences, as every second chain rotates 180° around the molecular chain axis, and the molecules are shifted by a distance equal to half of the c-axis lattice distance. These characteristics make the crystalline δ-phase polar with ferroelectric properties [15,17,18].

Even though PVDF is the second-most produced fluoropolymer [19], only a limited number of non-linear macromolecular architectures incorporating PVDF blocks have been described [20]. The reason for this is the relative scarcity of controlled polymerization techniques applicable to vinylidene fluoride (VDF). For example, the reversible addition-fragmentation transfer (RAFT) polymerization, with carefully chosen chain transfer agents, is compatible with VDF [21–25]. Several studies reported well-defined PVDF and its block-copolymers produced *via* iodine transfer polymerization (ITP) [26], and few of them deal with cobalt-mediated radical polymerization [27]. Very few PVDF-based branched architectures have been described, even though star polymers and brushes could be designed with a range of valuable and unique properties [28,29]. In particular, PVDF miktoarm star polymers could give rise to complex self-assembly behaviors and structural diversity beyond that of simple block copolymers [30–32].

The β-phase of PVDF has been the subject of many investigations. In the case of linear PVDF-homopolymer, stretching and corona poling have been used to enhance its piezoelectric constant [33–35]. Also, annealing and stretching processes in films at high temperatures have been employed for a similar purpose [36]. Blends of PVDF and other polymers have also been used to promote β-phase formation. PVDF/ PMMA (poly(methyl methacrylate)) blends have been reported as a way to obtain the much-desired PVDF β-phase [37,38]. In previous work, we have studied the crystallization of (polymethylene, equivalent to polyethylene) and PVDF blends (PM/PVDF), obtaining the crystallization of the ferroelectric β-phase and γ-phase during an isothermal crystallization or in a scan from the melt employing a slow cooling rate (1 °C/min) [39].

The crystalline β-phase has also been reported in PVDF-based random copolymers, for example in PVDF-*co*-PVA [(poly(vinyl alcohol)] that is crystallized in the β-phase independently of composition [40]. Another example is the P(VDF-*co*-TrFE) (trifluoroethylene), one of the most studied random copolymers, that also crystallizes directly in the all-trans conformation [41–44]. Furthermore, the crystalline β-phase has also been found in PVDF-based block copolymers. One of the important factors in obtaining the β-phase in this kind of copolymers is related to the morphology where confinement effects play an important role [45]. During the last years, in order to avoid the loss of capacity in energy storage applications, a series of graft copolymers based on poly(vinylidenfluoride-*co*-trifluoroethylene-*co*-cholorotri-fluoetoethylene) P(VTrCT) were synthesised [46]. Moreover, recent work has been published where β-phase crystallinity of PVDF homopolymer, blends and block copolymer with PMMA is induced by non-solvent crystallization [47].

In a recent work [48], María *et al.* demonstrated how chain topology in PVDF-*b*-PEO 4-miktoarm star copolymers influenced PVDF arms crystals' polymorphic behavior. This previous work showed that the miktoarm star chain topology induces the exclusive crystallization of the PVDF arms in the β-phase when the cooling rate is relatively low (i.e., at 1 °C/min).

In the present manuscript, we study the influence of isothermal crystallization conditions on the same 4-miktoarm star block copolymer samples employed in ref. 38. It should be noted that even though these copolymers were employed once before, their detailed synthesis pathway was not reported [48]. Hence, in this work, a full account of the synthesis of these novel miktoarm block copolymers is given.

Recent work has reported the isothermal crystallization of a linear PVDF homopolymer using a flash DSC equipment, which uses a cooling rate of 3000 °C/s to avoid any crystallization during cooling to the crystallization temperature. At crystallization temperatures between 60 and 65 °C, the formation of the β -phase was reported [49]. Isothermal crystallization experiments of PVDF films cast from solutions have also been studied, where PVDF in DMA solutions are cast on glass substrates and crystallized isothermally at 60 °C. In these films, the DMA helps the crystallization of PVDF completely in the polar β-phase [50]. This is unusual behavior in linear PVDF, in which normally the stable α-phase is formed when the sample is isothermally crystallized, and only in some isolated cases when the crystallization temperature is quite high, the γ-phase can be achieved [51].

The present work reports the detailed synthesis and isothermal crystallization study of the nucleation, spherulitic growth rates, and overall crystallization kinetics of novel complex 4-miktoarm star copolymers, previously used before by us to study the non-isothermal crystallization [48]. The application of different experimental techniques, such as Differential Scanning Calorimetry (DSC), Fourier Transform Infrared Spectroscopy **(**FTIR), and Polarized Light Optical Microscopy (PLOM), allow us to determine how these materials crystallize and which polymorphs can be formed. By determining nucleation, growth, and overall crystallization kinetics, we determine the parameters that affect the crystallization kinetics of the miktoarm star copolymers and evaluate the influence of chain topology and/or chain structure on polymorphic properties.

2. Experimental section

2.1. Materials and methods

Reagents and solvents used during the synthesis part of the manuscript were purchased from different chemical companies and used as received without any further purification. Dimethyl carbonate (DMC) (Sigma-Aldrich, ≥99%), dimethylformamide (DMF) (Sigma-Aldrich, 99.8%), acetonitrile (VWR, 99.8%), dichloromethane (VWR, 99.9%), tetrahydrofuran (THF) (Sigma-Aldrich, 99%), n-hexane (Alfa Aesar, 99.5%), ethyl acetate (VWR, 99%), triethylamine (Fisher Scientific,
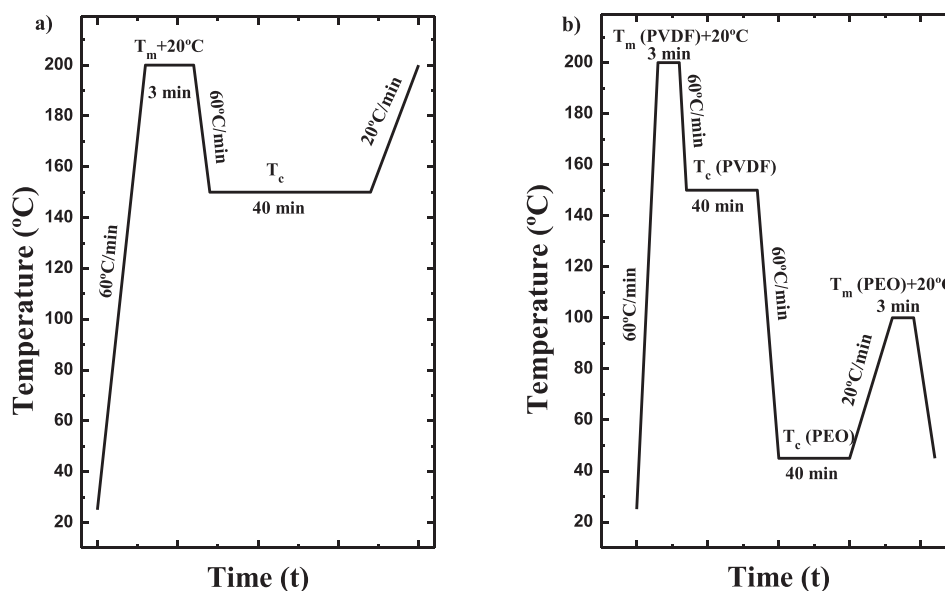
Fig. 1. Isothermal crystallization protocol, schematic representation of a) PVDF block crystallization and b) PEO block crystallization in the 4-miktoarm star block copolymers samples. To follow each step, see the text for a detailed description of the experimental procedure.

99%), sodium iodide (Sigma-Aldrich, 99.5%), sodium azide (Sigma-Aldrich, 99.5%), 2,2-bis(bromomethyl)propane-1,3-diol (Sigma-Aldrich, 99%), tetrakis(acetonitrile) copper(I) hexafluorophosphate (Sigma-Aldrich, 99.9%) and bis(t-butyl peroxy)cyclohexane (Sigma-Aldrich, 80%). 1,1-vinylidene fluoride was purchased from Apollo Scientific (≥98%) and used as it is. 1-*tert*-Butyl-4,4,4-tris(dimethylamino)-2,2-bis[tris(dimethylamino) phosphoranyli -denamino]-2λ5,4λ5-catenadi-(phosphazene) (*t*-BuP4, 0.8 M in hexane) and propargyl alcohol were supplied by Sigma-Aldrich and rediluted by an appropriate solvent (hexane or tetrahydrofuran) in a specific glass apparatus. Ethylene oxide (EO) (Sigma-Aldrich, 99.5%) was successively dried over calcium hydride and *n*-butyllithium (n-BuLi) before the polymerization.

2.2. Characterization techniques

2.2.1. Nuclear magnetic resonance Spectroscopy (NMR)

Several Bruker NMR instruments (AVQ 700 MHz, 600 MHz, 500 MHz, or 400 MHz) were employed to obtain ^{1}H, and ^{19}F spectra at 298 K. NMR chemical shifts are given in ppm. Residual solvent signals of CDCl$_3$ ([1]H δ 7.26, [13]C δ 77.16) were used for calibration.

2.2.2. Size Exclusion Chromatography (SEC)

Size Exclusion Chromatography (SEC) was employed to determine the average molar masses and their distribution (Đ). An Agilent liquid chromatography apparatus was used. It was equipped with two similar PL gel columns (5 μm, MIXED-C) connected in series with DMF as the mobile phase (1 mL/min). LiBr was added to DMF to make a 0.005 M solution. Two detectors were employed, namely a refractive index (RID) and a UV–Vis detector. The temperature of the column and flow path was controlled at 55 °C. Polystyrene samples were used as standards to construct the calibration curve. The GPC-Addon for ChemStation software (Agilent) was employed for data analysis.

2.2.3. Differential Scanning Calorimetry (DSC)

A Perkin Elmer DSC 8000 equipment fitted with an Intracooler II cooling system was used. Before DSC tests were carried out, a calibration with indium and tin was performed. Ultra-high purity nitrogen was employed as a purge gas.

The experimental protocol suggested by Lorenzo *et al.* [52] was used to determine the overall isothermal crystallization. First, the minimum isothermal crystallization temperature to be used was found. This was

done by heating the sample to 20 °C above its melting temperature for 3 min to ensure that the sample was completely melted, then it was cooled down at 60 °C/min to a chosen T_c and immediately heated up again to the molten state (at 20 °C/min). The lowest T_c, which does not generate any latent heat of fusion during a subsequent DSC heating scan, was selected as the minimum T_c used [52].

Fig. 1 shows schematically the steps carried out to perform isothermal crystallization. Samples were melted (20 °C above the melting temperature for 3 min) to remove any crystalline thermal history. From that temperature, they were cooled at 60 °C/min (at this cooling rate, the calorimeter has an excellent control of the temperature) to (as mentioned above) a previously chosen isothermal crystallization temperature, T_c. At this temperature, the samples were left to crystallize until saturation, around 40 min in all the samples. After the completed crystallization, a heating scan was carried out at 20 °C/min until melting to study the polymorphic nature of the isothermally produced crystals (Fig. 1a).

For the 4-miktoarm star block copolymer samples, when we wanted to study the the PEO phase, a preliminary first step was carried out to crystallize the PVDF phase to saturation as it crystallizes at higher temperatures than PEO blocks, as it is shown schematically in the Fig. 1b. Once the PVDF blocks are crystallized, a second isothermal crystallization process is carried out at different chosen T_c values. Hence, during the PEO blocks overall isothermal crystallization process, the PVDF component is always semi-crystalline. All the kinetic calculations were performed with the complimentary Origin® plugin developed by Lorenzo *et al.* [52].

2.2.4. Fourier Transform Infrared Spectroscopy (FTIR)

A Thermo Scientific Nicolet 6700 instrument, equipped with a nitrogen purge and aligned for signal clarity, was employed to collect the data for the synthesis part of the manuscript. Acetone cleaned and dried crystal surface was used for calibration before sampling; up to 512 scans (from 4000 to 550 cm^{-1}) were taken for each sample and background.

Moreover, a Nicolet 6700 FTIR fitted with an ATR (Attenuated Total Reflectance) Golden Gate MK II system with a diamond crystal was used to test the 4-miktoarm star block copolymer samples. Film samples were prepared by first melting bulk samples at 200 °C for 3 min and then cooled them down at 60 °C/min to 150 °C to allow their crystallization at this temperature for 2 h. Finally, the samples were cooled down again at a controlled cooling rate of 20 °C/min until room temperature. For all
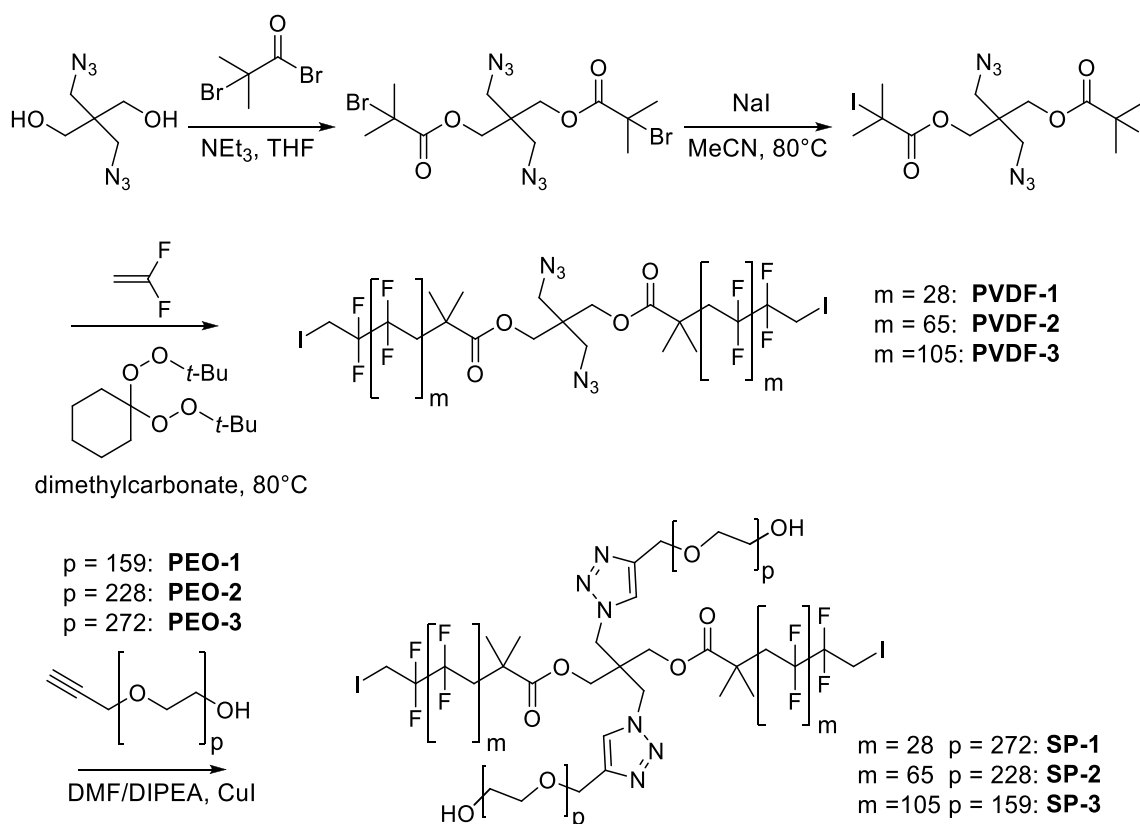
Fig. 2. Synthesis of (PVDF)$_2$(PEO)$_2$ miktoarm star copolymers.

Table 1

Molecular characteristics of the samples synthesized and studied in this work.

Sample	Topology	PVDF/PEO ratio (wt%/wt%)[a]	M_n (g/mol)[b]	M_n PVDF (g/mol)[b]	M_n PEO (g/mol)[b]	Đ[c]
(PVDF$_{29}$-N$_3$)$_2$	2-arm (linear)	1/0	3800	3800	–	1.23
PEO$_{227}$-Alkyne	1-arm (linear)	0/1	10,000	–	10,000	1.10
(PVDF$_{29}$)$_2$(PEO$_{272}$)$_2$	4-arm (miktoarm)	13/87	27,800	3800	24,000	1.11
(PVDF$_{66}$)$_2$(PEO$_{227}$)$_2$	4-arm (miktoarm)	29/71	28,500	8500	20,000	1.13
(PVDF$_{106}$)$_2$(PEO$_{159}$)$_2$	4-arm (miktoarm)	48/52	27,900	13,900	14,000	1.13

[a] Based on PVDF and PEO M_n values. [b] Estimated from ^{1}H NMR integration. [c] Acquired from SEC analysis (Figure S20). Due to the non-linear baseline, these values are underestimated.

these sample preparation processes, an external Linkam hot-stage was employed. FTIR experiments were performed at room temperature.

2.2.5. Polarized Light Optical Microscopy (PLOM)

Polymer films were examined with an Olympus BX51 polarizing microscope, fitted with a hot-stage (Linkam) and a liquid N$_2$ system to control the cooling rate and temperature. An Olympus SC50 camera was used to take images. The samples were prepared by the drop-casting method. Solutions (at 4 wt%) containing either the precursors or block copolymers in DMF solvent were drop cast on glass substrates and dried in a heater before observing them under the microscope. The isothermal crystallization experiments are carried out following the same protocol explained before for DSC experiments.

3. Results and discussion

3.1. Polymer synthesis

The synthesis of the bifunctional iodine transfer polymerization (ITP) agent containing the N$_3$(C$_3$)N$_3$ "clickable" moiety and of the miktoarm star copolymers, are given in Fig. 2. Polymerization of VDF using ITP as chain transfer agent and bis(*tert*-butyl peroxy)cyclohexane as initiator yielded the linear polymers **PVDF-1, PVDF-2, and PVDF-3** with two 1,3-diazide groups at the middle of the PVDF chains. The molar mass of the resulting polymers was checked by SEC and NMR spectroscopy. SEC analyses used linear polystyrenes as standard. The molar mass determined by SEC for star fluoropolymers would underestimate the real molar masses because of differences in hydrodynamic volume with the corresponding linear polymer and, thus different elution times. Hence, the Đ was determined by SEC, and ^{1}H NMR spectroscopy was used to calculate the molar masses of polymers. The molecular characterization data for these samples are given in Table 1. Synthetic details of the transfer-agent, ITP, ω-alkyne-PEO, and "click" reaction are reported in the Supporting Information (SI). NMR and IR spectra and SEC traces of all intermediate and final products are given in the SI (Figure S1, S2, S5-S19, and S22-S23).

For all polymerizations, the dependence of VDF conversion *vs.* time and molar mass *vs.* time appeared to be linear (Figures S3 and S4). This might indicate a constant concentration of active chain ends during polymerization up to a certain degree of conversion and proves that the
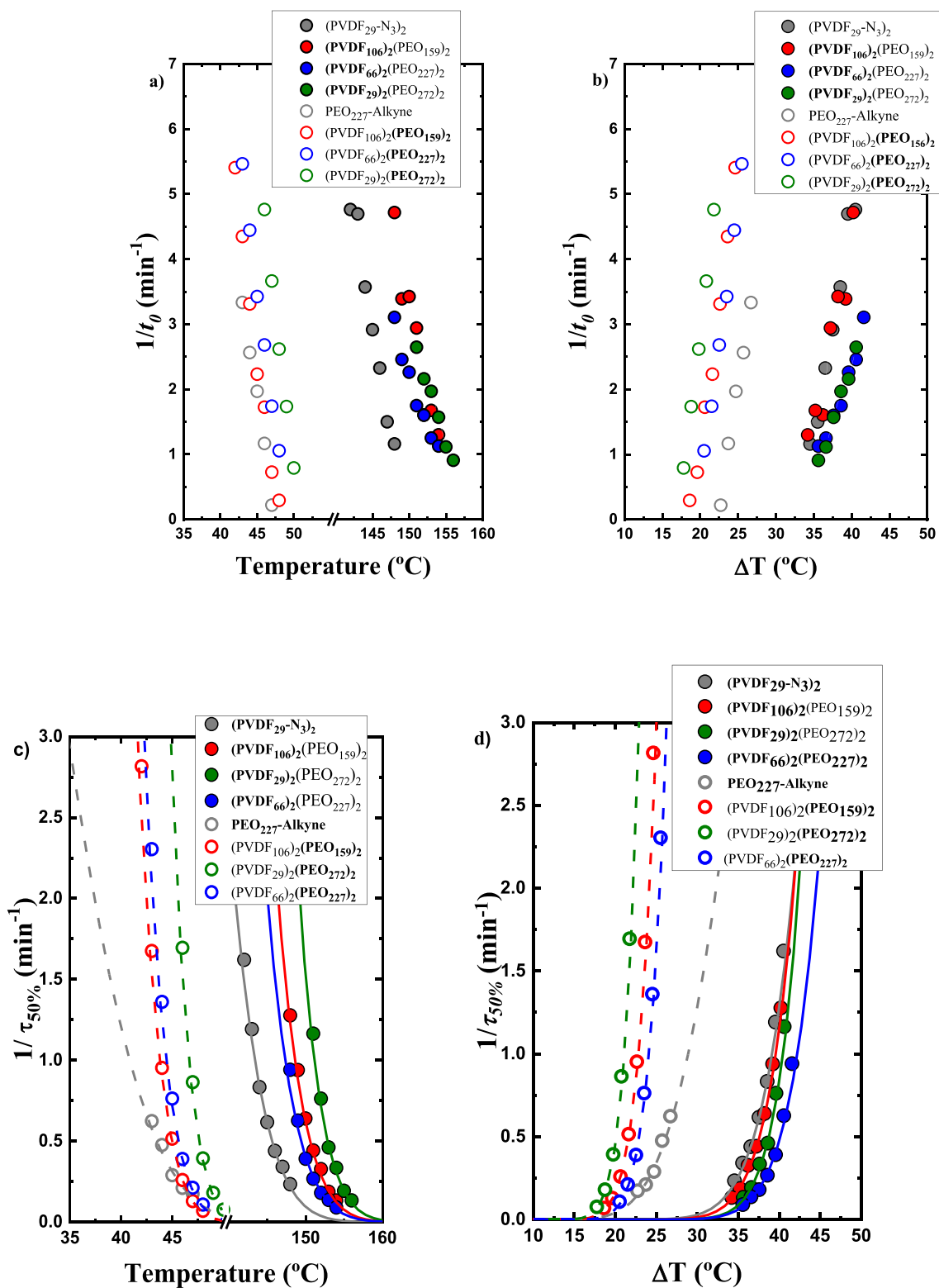
Fig. 3. Inverse of the induction time (t_0) obtained by DSC versus a) the crystallization temperature and b) the supercooling for PVDF precursor, PEO precursor, $(PVDF_{106})_2(PEO_{159})_2$, $(PVDF_{29})_2(PEO_{272})_2$ and $(PVDF_{66})_2(PEO_{227})_2$ samples. Inverse of half crystallization time ($1/\tau_{50\%}$) as a function of c) isothermal crystallization temperature and d) the supercooling for PVDF precursor, PEO precursor, $(PVDF_{106})_2(PEO_{159})_2$, $(PVDF_{29})_2(PEO_{272})_2$ and $(PVDF_{66})_2(PEO_{227})_2$ samples. All the solid lines are fit according to the Lauritzen and Hoffman theory. The dashed and solid lines were obtained by fits to the Lauritzen and Hoffmann theory.

chosen chain transfer agent is adequate for VDF polymerization control in agreement with the previous report [26,27].

The preservation of the azides under the employed polymerization conditions was confirmed by FTIR (Figure S22). To prove the symmetrical character of the $(PVDF)_2$ polymer, we cleaved the ester central bonds by hydrolysis. The comparison of the M_n values before (M_{nSEC} = 19000 Da) and after hydrolysis (M_{nSEC} = 10000 Da), and the consistent Đ values (Figure S21), suggests that the reactivity of the

bifunctional chain transfer agent was similar for the two iodides.

The azide-functionalized **PVDF-1, PVDF-2, and PVDF-3** were then reacted with complementary alkyne-functionalized poly(ethylene oxide) **PEO-1**, **PEO-2**, and **PEO-3** to yield star polymers **SP-1**, **SP-2** and **SP-3**. The molar masses of the PEO and PVDF blocks were varied. Because of the peculiar mechanism of CuAAC discovered by Finn et al [53], both azides of the $N_3(C_3)N_3$ moiety react simultaneously, with a complete absence of mono-triazole intermediate. This property of CuAAC is most convenient as it prevents the need for purification to separate the four-arm miktoarm star from the incompletely-reacted three-arm intermediate, as an excess of PEO-alkyne is not required. FTIR was employed to monitor the reaction by the disappearance of band at 2095 cm^{-1}, which is due to the azide (Figure S22). The diblock polymer star displayed a narrower apparent $Đ$ value by SEC than that obtained for linear $(PVDF)_2$ (Table 1 and Figure S20). SEC-estimated $Đ$ usually decreases in the transition between linear and branched macromolecules, because branching reduces the polymer hydrodynamic volume and significantly impacts the distribution of the hydrodynamic sizes.[54] Finally, three PVDF (3700, 8500, and 13600 g/mol) and three ω-alkyne-PEO (14000, 20000, 24000 g/mol) were synthesized.

In summary, the three $(PVDF)_2(PEO)_2$ star block copolymers studied here have similar molar masses, and PVDF/PEO ratios are 0.15, 0.41, and 0.92. To compare with the 4-miktoarm star block copolymers, the $(PVDF_{29}-N_3)_2$ ($M_n = 3700$, $Đ = 1.23$), and PEO-alkyne ($M_n = 10000$, $Đ = 1.10$) precursors were also analyzed.

3.2. Isothermal crystallization kinetics

In a previous publication, we have already discussed the miscibility between PVDF and PEO [48]. After using SAXS (Small Angle X-ray Scattering) and PLOM techniques and employing the Flory-Huggins theory [55], we concluded that in the molten state, these polymers are miscible or weakly segregated.

The determination of the crystallization kinetic parameters for PVDF and PEO blocks in every sample was carried out. When the PVDF blocks are crystallized, the PEO blocks are still in the molten state. On the other hand, to calculate the kinetic parameters of PEO blocks, first, the PVDF blocks are crystallized to saturation, and subsequently, the PEO blocks are crystallized.

Fig. 3a and 3b show the inverse of the induction time (t_0), a quantity proportional to the primary nucleation rate before the crystallization process has started. This nucleation rate of the PVDF and PEO blocks is plotted for all samples as a function of the crystallization temperature (T_c) and the supercooling ($T_m^0 - T_c$), respectively. The two PVDF arms of the 4-miktoarm star block copolymers have nucleation rates that are higher than that of the 2-arm linear PVDF precursor, a peculiar effect as the PEO arms in the stars are in the melt when the PVDF arms nucleate. Similarly, the PEO precursor shows a lower nucleation rate in comparison to the PEO arms within the stars. To observe better the difference in the nucleation rate values, Figures S24 and S25 (in the SI) show the values of $1/t_0$ at constant T_c and $\triangle T$ values for the PEO and PVDF, respectively. The estimation of the equilibrium melting temperature (T_m^0) for each sample using the Hoffman-Week method (Figure S26) is explained in the SI, and the values are shown in Table S2. These values extrapolated by the Hoffman-Weeks method are employed to fit the data presented in Fig. 3c and 3d with the Lauritzen and Hoffman theory. We were not able to identify a unifying trend in the three different star copolymers with respect to their composition.

Fig. 3c and 3d plot overall crystallization rates (i.e., the inverse of the half crystallization time ($1/\tau_{50\%}$)), versus T_c and the supercooling for all the materials examined. The curves plotted as a function of supercooling are closer to each other, but there is not a perfect superposition between copolymers and their homopolymers. This result indicates the predominance of kinetic factors over the thermodynamic normalization attempted by plotting the curves as a function of supercooling. The trends observed in Fig. 3c and 3d are qualitatively similar to those
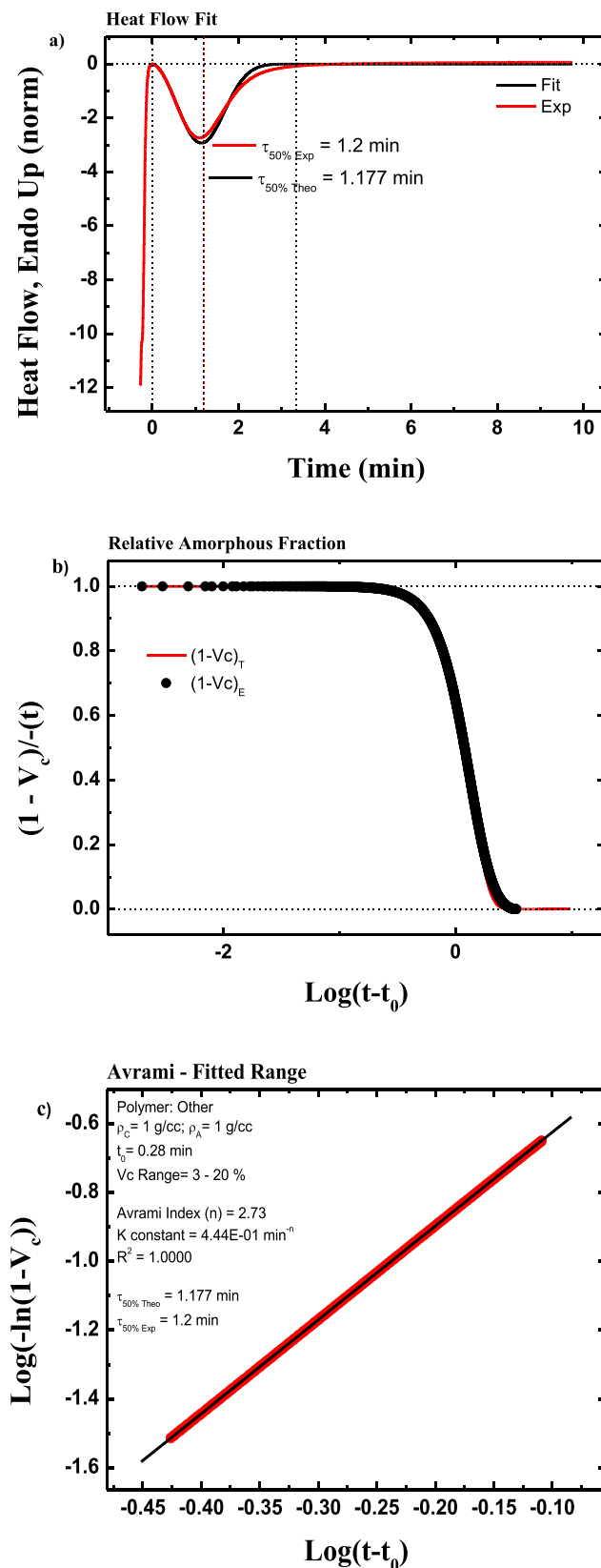

Fig. 4. (a–c) The fit to the Avrami equation using the origin plug-in developed by Lorenzo *et al.* compared to the DSC experimental data obtained for the $(PVDF_{29}-N_3)_2$ sample [52].
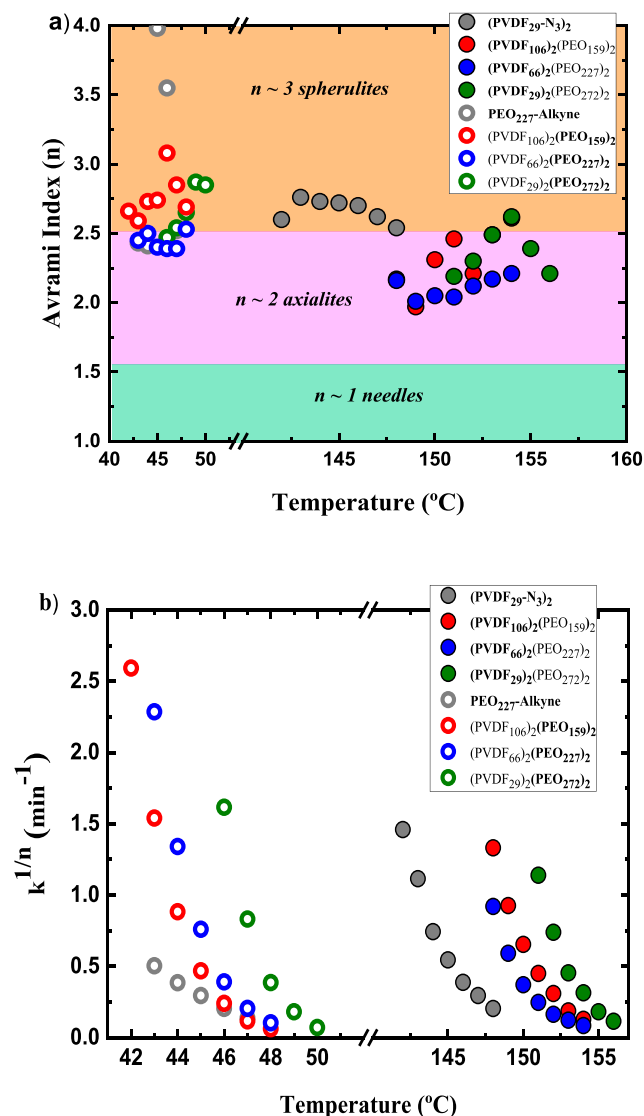
Fig. 5. a) Avrami index values as a function of the crystallization temperature and b) normalized isothermal crystallization rate constant of the Avrami model as a function of crystallization temperature for all the samples studied.

observed in Fig. 3a and 3b, indicating that nucleation is a dominant factor for the overall crystallization behavior of the materials (that includes nucleation and growth contributions). Figures S27 and S28 in the SI plot data from Fig. 3c and 3d at constant T_c and $\triangle T$ values for PEO and PVDF, respectively.

In summary, both the nucleation rate and the overall crystallization rates of the PVDF and PEO arms within the 4-miktoarm star block copolymers are higher than those of their precursors. The nucleation effects dominate the overall crystallization kinetics.

The Avrami equation describes well the primary crystallization in polymers [56]. One of the possible ways to write the equation is [52,57]:

$$1 - V_c(t - t_0) = exp\left(- k(t - t_0)^n\right) \qquad (1)$$

where V_c is the relative volumetric transformed fraction, t_0 is the induction time before any crystallization has started, t is the experimentally determined time, k is the overall crystallization rate constant, and n is the Avrami index. The Avrami index depends on the nucleation rate and crystal growth geometry.

One example of the excellent agreement between the experimental data and the Avrami prediction theory in the primary crystallization range is represented in Fig. 4 (i.e., until 50% relative crystallization).

The n value obtained for the $(PVDF_{29}-N_3)_2$ was 2.7, this value can be considered to be close to 3. This is indicative that the PVDF arms have crystallized with instantaneously nucleated spherulites. Fig. 4a shows a comparison between an experimentally determined DSC isotherm and the one predicted by the Avrami theory.

Fig. 4c demonstrates that the fitting to the Avrami equation can predict the primary crystallization range overall kinetics of the PVDF arms (the correlation coefficient is 1.0000), before the spherulites touch one another (i.e., free growth regime), in a crystallization range up to 25% relative conversion from the melt to the semi-crystalline state. Moreover, as it can be seen in Fig. 4a and 4b the fits are good in this case for PVDF up to much higher relative conversion to the semi-crystalline state (i.e., until 50%, as given by the good agreement between the experimental and predicted half-crystallization times).

Through the Avrami equation fit (Fig. 4c), the Avrami index (n) is calculated for every temperature chosen during the isothermal crystallization. The Avrami index values are plotted in Fig. 5a against the crystallization temperature. The values of the Avrami index fluctuate between 2 and 3. If the studied block is PEO for the copolymers, the Avrami index is closer to 3 (instantaneous nucleated spherulites). On the other hand, if the studied block is PVDF, it is closer to 2 (instantaneous nucleated axialites) with the exception of the homopolymer, whose n values are closer to 3.

Fig. 5b shows the crystallization temperature dependence of $k^{1/n}$ values. These values obtained by the Avrami fit for $k^{1/n}$ are proportional to the overall crystallization rate constant (whose excellent fit is given up to 25% relative conversion to the semi-crystalline state by the free growth of spherulites or axialites) in normalized units of min^{-1} (thanks to elevating k to the power $1/n$, as the units of k are given as $time^{-n}$). This is a good way to compare the Avrami predictions (plotted as data points in Fig. 5b) with the experimental values obtained during the isothermal crystallization experiments (experimental values of $1/\tau_{50\%}$ in Fig. 3c). In Fig. 5b, the comparison between the experimental data and the Avrami fit predictions are made at 50% relative crystalline conversion. This means that in the experimental case, impingement between spherulites would have probably started, especially when the nucleation is not perfectly instantaneous. This explains why there is a qualitative agreement between Fig. 5b and Fig. 3c, but there are some quantitative differences.

3.3. Melting processes observed after the isothermal crystallization procedures of the precursor homopolymer samples studied by DSC

This section analyzes the melting process after isothermally crystallized samples are heated in the DSC (starting at their corresponding T_c values), registering their melting behavior. Fig. 6 shows the DSC heating scans at 20 °C/min after each isothermal crystallization process for the $(PVDF_{29}-N_3)_2$ and PEO_{227}-Alkyne samples. In the case of the $(PVDF_{29}-N_3)_2$ homopolymer (Fig. 6a), the temperature range chosen for the isothermal crystallization study was 142–152 °C, and for the PEO_{227}-Alkyne homopolymer (Fig. 6b), the temperature range was 43–50 °C.

In the case of PEO (Fig. 6b), the main melting peak is observed at approximately 62 °C, this peak increases as the crystallization temperature increases as expected. We will not address the behavior of the PEO precursor in detail, as the main objective of this work is to investigate the polymorphic behavior of PVDF.

Fig. 6a shows the melting behavior of the $(PVDF_{29}-N_3)_2$ precursor (a linear 2-arm PVDF sample). Different melting peaks are observed due to the different polymorphic phases detected in PVDF. The isothermal crystallization peaks at the different crystallization temperatures are plotted in Figure S29 of the SI for both samples.

According to the literature, commercial PVDF homopolymers exhibit only one phase when isothermally crystallized from the melt, specifically the α- non-polar phase [58,59]. In our case, in the synthesized $(PVDF_{29}-N_3)_2$ precursor, at low isothermal crystallization temperatures ($T_c = 142$ °C), two melting peaks can be distinguished. The first one
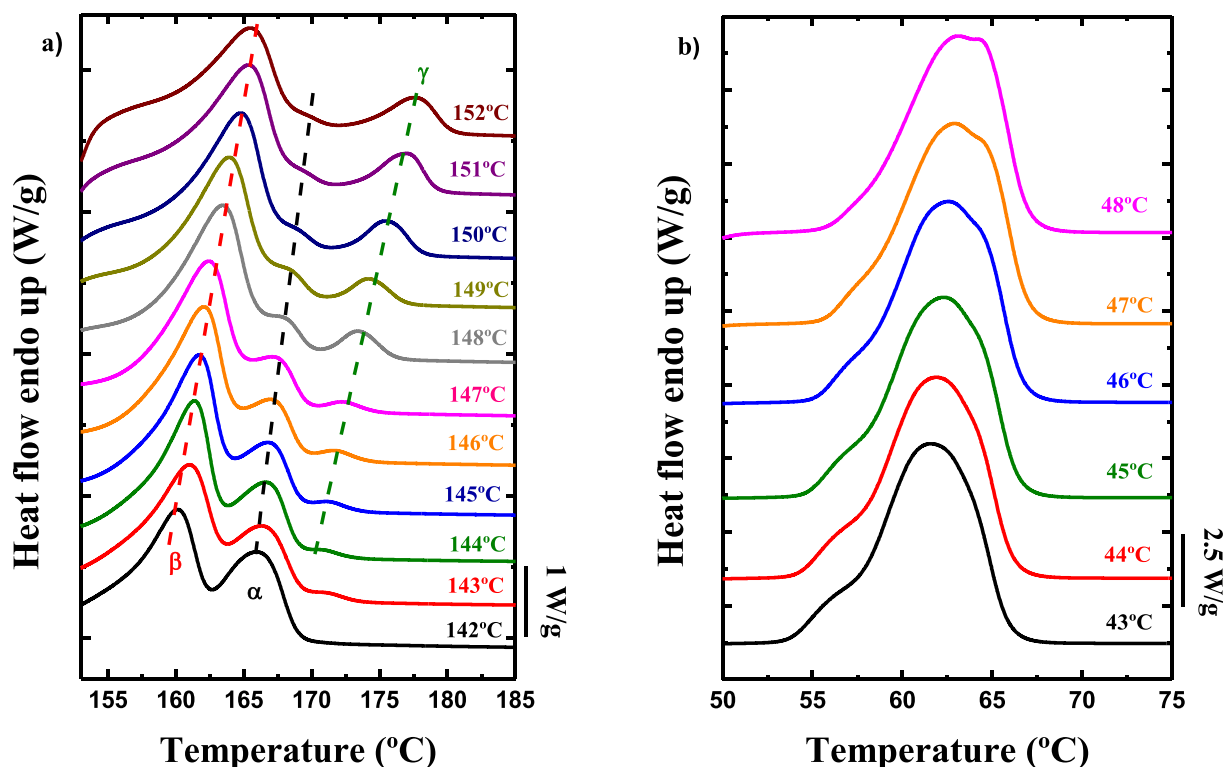
Fig. 6. DSC heating scans at 20 °C/min after the samples were isothermally crystallized for 40 min at the indicated temperatures: a) (PVDF$_{29}$-N$_3$)$_2$ and b) PEO$_{227}$-Alkyne precursor samples.
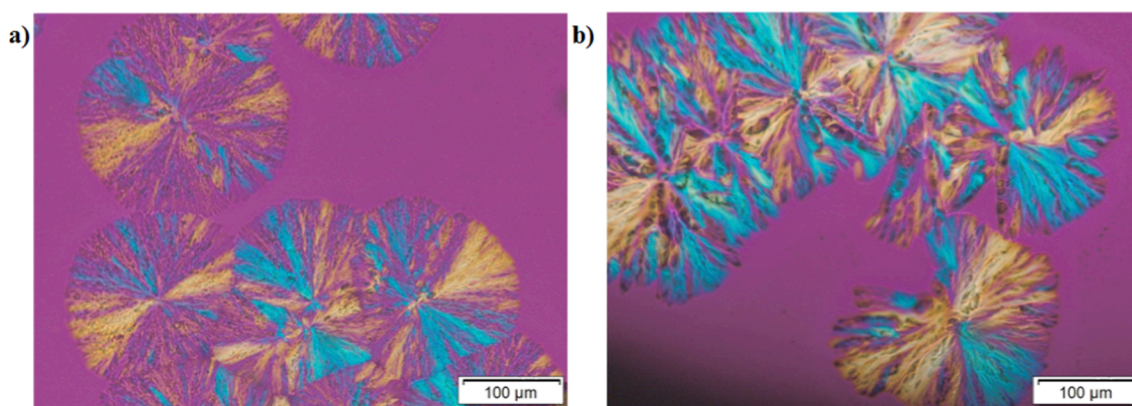

Fig. 7. PLOM micrographs of (PVDF$_{29}$-N$_3$)$_2$ spherulites isothermally crystallized a) at 146 °C and b) at 157 °C from the melt.

appears at low temperatures, and can be assigned to the less stable crystalline β-phase. The second one, at higher temperatures, corresponds to the melting of α-phase crystals. When the isothermal crystallization temperature increases, the α-phase melting peak area decreases, and a new peak can be observed at higher temperatures. This peak corresponds to the melting of a new crystalline phase crystals, which can be assigned to the γ-phase. At the highest isothermal crystallization temperature (T_c = 152 °C), the α-phase crystals have almost disappeared, and both β-phase and γ-phase coexist. A possible explanation may be that a transition from the α-phase to the γ-phase occurs during the isothermal crystallization process, as it has been observed before in the literature when the isothermal crystallization temperature selected is high enough [60,61]. These type of transitions have been previously reported for PVDF nanocomposite samples but has never been reported before for PVDF-based block copolymer samples [62–64]. In the present work, the (PVDF$_{29}$-N$_3$)$_2$ homopolymer precursor is not equal to a

commercial PVDF homopolymer, as it has a more complex structure being a 2-arm copolymer, see its chemical structure in Scheme S1 (i.e., **PVDF-1**).

A morphological study was carried out by PLOM. Fig. 7 shows micrographs of the (PVDF$_{29}$-N$_3$)$_2$ precursor taken at two different isothermal crystallization temperatures that complement the DSC results. Fig. 7a presents some PVDF spherulites grown at 146 °C after 3 min at this temperature, where the main phase observed by DSC was the β-phase. On the other hand, Fig. 7b shows spherulites grown at 157 °C during 10 min on the same sample where the main phase observed by DSC was the γ-phase. Differences in texture are detected in both cases, where the γ-phase crystals observed in Fig. 7b are more compact and dense than the β-phase crystals observed in Fig. 7a. Therefore, depending on the isothermal crystallization temperature employed, it is possible to observe two types of spherulites in the same sample. In the literature, some works have found similar differences in the texture of
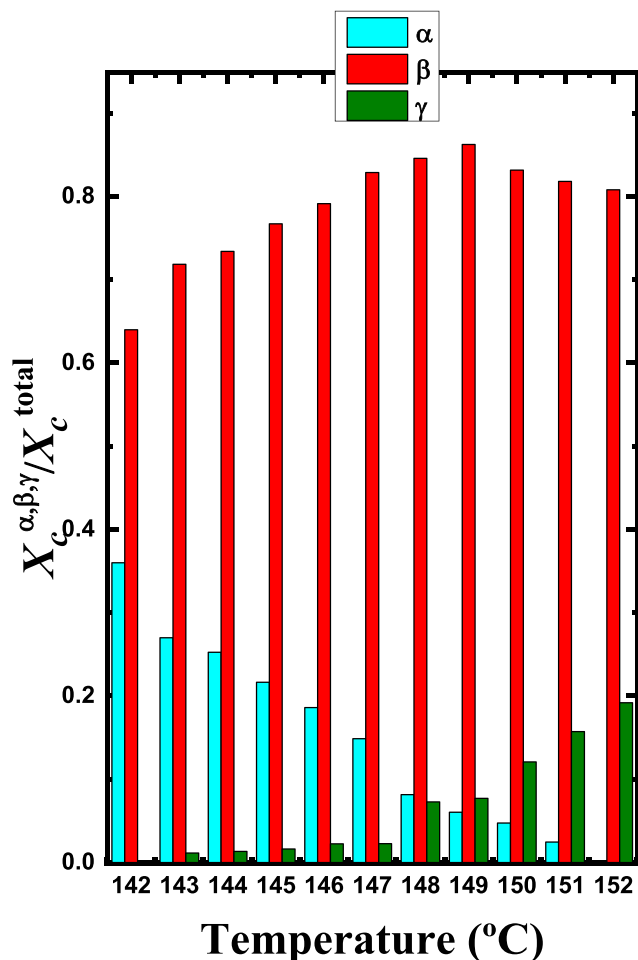
Fig. 8. Degree of crystallinity of each phase divided by the total degree of crystallinity at all the isothermal crystallization temperatures studied.

PVDF spherulites depending on the crystalline phase that is being formed [51,65–67].

As explained before, the α-phase to γ-phase transition is a well-known process in the literature [68–70]. Normally, this conversion process requires long crystallization times, but in our case, as we have confirmed before, due to the topological effects of the 2-arm chain conformation in this PVDF precursor, this α-γ phase transition occurs with the increase of the crystallization temperature, even at short crystallization times. The chain topology influences the final properties of the sample, as we demonstrated in miktoarm star structures before [48].

To understand how the α-phase changes to γ-phase, different calculations were performed. Three different hypotheses will be discussed: (i) a direct transition from α-phase crystals to γ-phase crystals during the duration of the isothermal crystallization, (ii) the α-phase, that is first formed, melts (during isothermal crystallization) and the γ-phase forms from this melt state, as the crystallization temperature increases and (iii) the β-phase, that is first formed, melts, and then the γ-phase crystallizes from this melt state. To study these different possibilities, some calculations are carried out and are presented in Fig. 8.

Fig. 8 presents a plot of the degree of crystallinity of each Phase $(X_c^{\alpha,\beta,\gamma})$ divided by the total degree of crystallinity (X_c^{total}) for each isothermal crystallization temperature.

$X_c^{\alpha,\beta,\gamma}$ is calculated from the melting enthalpy data obtained by DSC analysis (Eq. (2)), and X_c^{total} value is obtained by the sum of all the crystallinity degrees (Eq. (3)):

Table 2
List of the values in percentage of each phase crystallized in the $(PVDF_{29}\text{-}N_3)_2$ at every isothermal crystallization temperature.

T_c (°C)	α-phase (%)	β-phase (%)	γ-phase (%)
142	36	64	0
143	27	72	1
144	25	73	2
145	21	77	2
146	18	79	3
147	15	82	3
148	8	84	8
149	6	86	8
150	5	83	12
151	2	82	16
152	0	81	19

$$X_c = \frac{\Delta H_m}{\Delta H_m^0 * \varphi} \tag{2}$$

$$X_c^T(T) = X_c^\alpha(T) + X_c^\beta(T) + X_c^\gamma(T) \tag{3}$$

where ΔH_m is the experimental latent heat of fusion measured in the DSC, ΔH_m^0 is the equilibrium melting enthalpy (i.e, for a 100% crystalline sample), and φ is the weight fraction of the polymer. For the PVDF we have employed a value of $\Delta H_m^0 = 104.7$ J/g [71]. The explanation of how we calculate the degree of crystallinity and how we obtain the separate melting enthalpies are in the SI (Figure S30).

Fig. 8 shows how the β-phase is almost constant in the whole range calculated; thus, we can estimate that the β-phase does not melt as the isothermal crystallization temperatures are increased and always remains crystalline, so hypothesis (iii) can be rejected. For the α-phase, the value of the degree of crystallinity decreases when the crystallization temperature increases, and at the same time, the degree of crystallinity for the γ-phase increases. In addition, the β-phase is not changing with crystallization temperature, as the total crystallinity observed remains almost constant, so hypothesis (ii) can also be rejected. Fig. 8 thus demonstrates that there is a direct crystalline phase transition from α-phase to γ-phase in the $(PVDF_{29}\text{-}N_3)_2$ sample during the isothermal crystallization process. The content of each phase (in %) at every isothermal temperature employed are listed in Table 2.

3.4. Melting processes observed after the isothermal crystallization procedures of the PVDF arms within the 4-miktoarm star block copolymer samples studied by DSC

The melting of the PVDF arms crystals within the $(PVDF)_2(PEO)_2$ 4-miktoarm star block copolymers was also studied after isothermal crystallization by DSC. Fig. 9 shows the DSC heating curves of the miktoarm star block copolymer samples at 20 °C/min for the PVDF blocks after their isothermal crystallization for 40 min at different T_c values. The respective DSC cooling curves are shown in Figure S31 in the SI.

The behavior of the PVDF arms within the 4-miktoarm star block copolymers is remarkable. A single melting peak (whose peak value increases as T_c increases as expected) can be observed in Fig. 9 for all three samples. A single melting peak is observed in all samples regardless of the isothermal crystallization temperature employed or the miktoarm star copolymer composition selected. Compared to the PVDF precursor studied, this melting peak means that the copolymers, regardless of the sample studied, always crystallize in one crystalline phase. To determine which phase is this, FTIR analyses were carried out.

The three 4-miktoarm star block copolymers were isothermally crystallized at 150 °C for 2 h and finally cooled down at 20 °C/min to room temperature before the FTIR spectra were measured. Fig. 10a shows the FTIR results for the copolymers, crystallized all of them at the same temperature, and Fig. 10b shows the PEO_{227}-alkyne precursor
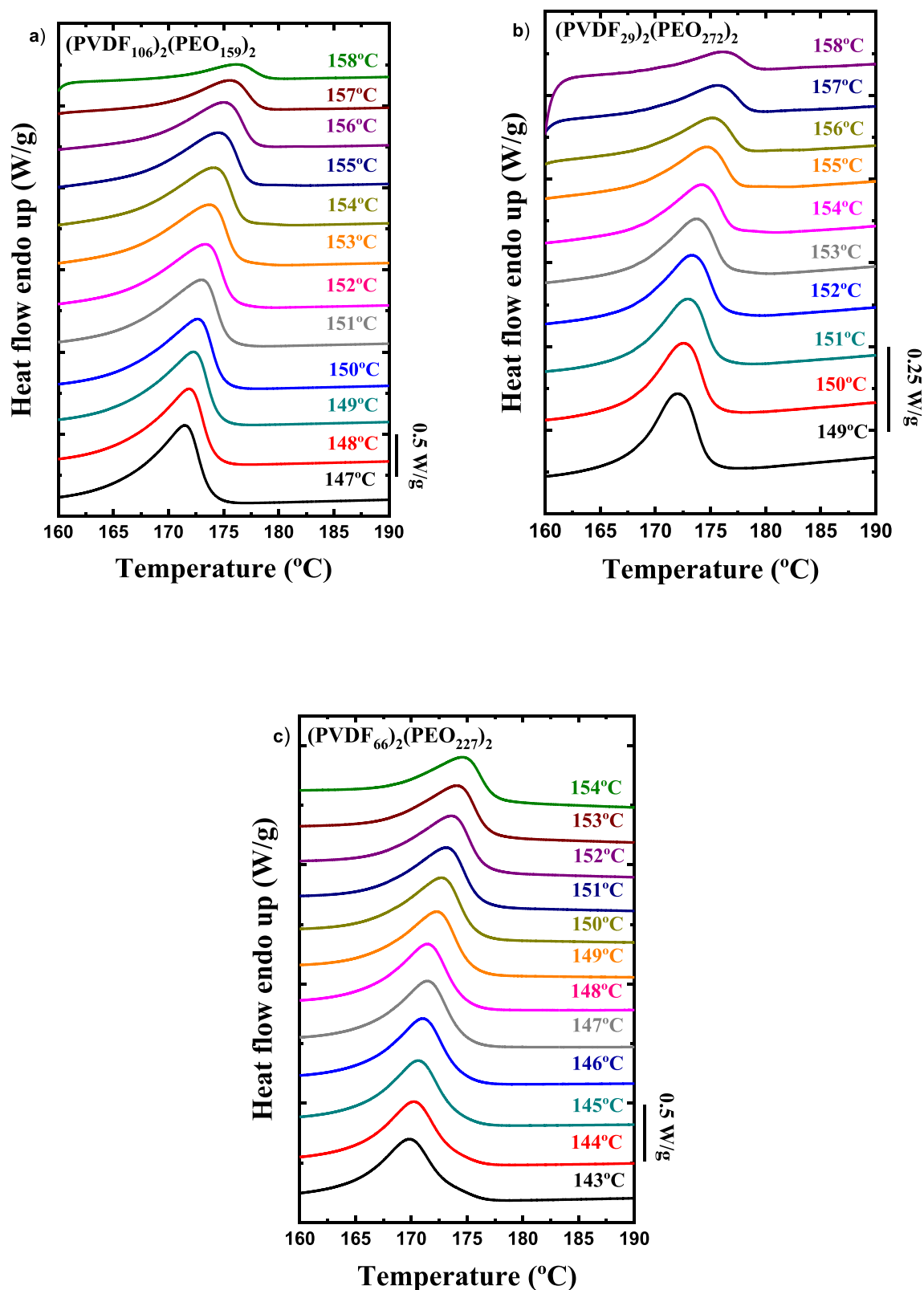
Fig. 9. DSC heating scans after 40 min isothermal crystallization at the indicated temperatures for the PVDF arms of the following samples: a) $(PVDF_{106})_2(PEO_{159})_2$, b) $(PVDF_{29})_2(PEO_{272})_2$ and c) $(PVDF_{66})_2(PEO_{227})_2$.

sample to observe and compare the possible interferences with the PVDF bands.

Fig. 10a shows some characteristic bands for $(PVDF_{106})_2(PEO_{159})_2$, $(PVDF_{29})_2(PEO_{272})_2$, and $(PVDF_{66})_2(PEO_{227})_2$ samples. As expected,

considering the melting temperature range observed by DSC, the bands detected in the FTIR spectra for the PVDF arms are related to the crystalline β-phase. The FTIR spectra shown here are just focused in the range of 1600–600 cm^{-1}, where all the PVDF characteristic bands
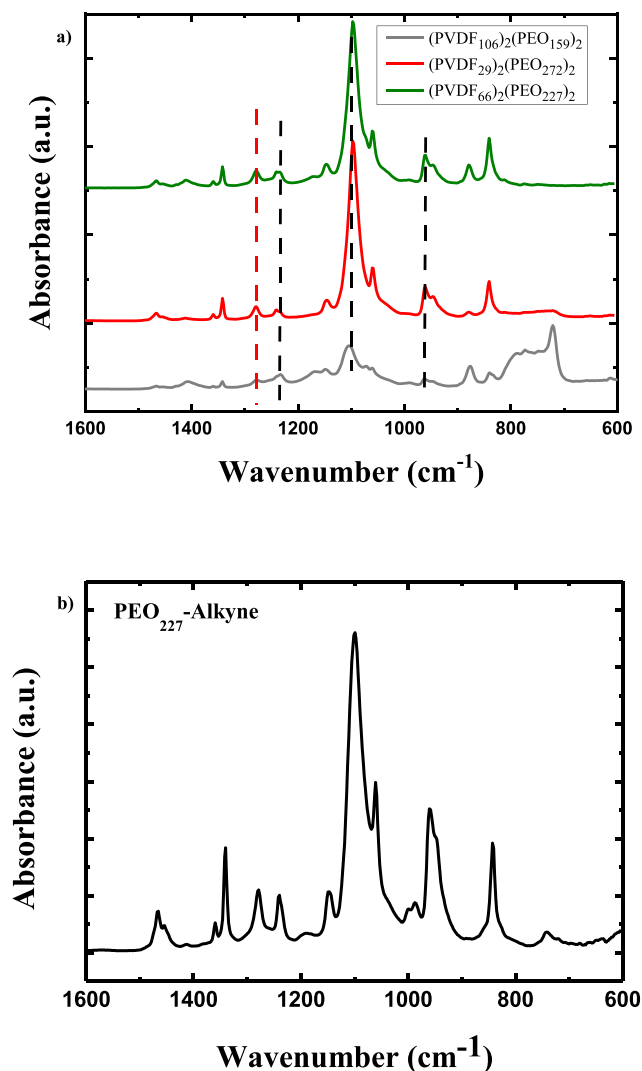
Fig. 10. FTIR spectra for a) $(PVDF_{106})_2(PEO_{159})_2$, $(PVDF_{29})_2(PEO_{272})_2$ and $(PVDF_{66})_2(PEO_{227})_2$ samples where PVDF was isothermally crystallized at 150 °C during 2 h and b) PEO_{227}-Alkyne homopolymer crystallized isothermally at 44 °C. The different vertical dashed lines indicate the bands for the PVDF and PEO. Black: PEO. Red: PVDF β-phase. (For interpretation of the references to colour in this figure legend, the reader is referred to the web version of this article.)

Table 3
Main location and description of the PVDF bands for the α, β, γ-phases and PEO bands in FTIR analysis.

Wavenumber (cm^{-1})	Phase	Description [16,74]
764	α-PVDF	C-C in-plane rocking vibration
796	α-PVDF	CH$_2$ rocking
833	γ-PVDF	–
840	β-PVDF	CH$_2$,CF$_2$ asymmetric stretching vibration
841	PEO	CH$_2$ wagging
960	PEO	CH$_2$-CH$_2$ rocking
976	α-PVDF	CH out of plane deformation
1100	PEO	C-O-C stretching
1232	γ-PVDF	CF out of plane deformation
1275	β-PVDF	CF out of plane deformation

appear. The bands located at 1238, 1101, and 961 cm^{-1} are the main bands detected for the PEO [72], as observed in Fig. 10b. It is worthy to say that there is a band located at 840 cm^{-1} that overlaps the crystalline β-phase in PVDF with one of the PEO bands. In Fig. 10a for the PVDF

blocks, there is a single band located at 1275 cm^{-1}. This band is characteristic for the β-phase [73], and was also observed before in our previous work in these systems [48]. It is remarkable that after the isothermal crystallization of these miktoarm block copolymers only the β-phase was formed. In fact, all characteristic bands from the α-phase (764, 796, and 976 cm^{-1}) are absent. Moreover, the bands corresponding to the γ-phase (833 and 1232 cm^{-1}) are also not observed. Table 3 shows all the main bands related to the PEO and for the different PVDF polymorphic phases. The results presented here are strong evidence indicating that the PVDF arms within the 4-miktoarm star block copolymers crystallize only in the β-phase when the samples are isothermally crystallized from the melt.

When these block copolymers samples are observed in the PLOM during an isothermal crystallization at high temperatures, it is possible to follow the crystallization of the PVDF arms. For the $(PVDF_{29})_2(PEO_{272})_2$ sample, the small amount of PVDF prevents the observation of PVDF block crystals in the microscope. Fig. 11 shows the PVDF arms crystals obtained for $(PVDF_{66})_2(PEO_{227})_2$ (Fig. 11a) and $(PVDF_{106})_2(PEO_{159})_2$ (Fig. 11b) respectively, at a crystallization temperature of 140 °C. In micrograph 11a, the PVDF arms crystals have a morphology in between spherulites and axialites. However, when the amount of PVDF in the star copolymers is the highest, as shown in Fig. 11b, the crystals formed by the PVDF arms are clear negative spherulites. In both cases, the crystals observed are consistent with PVDF β-phase morphology.

4. Conclusions

Novel A_2B_2 PVDF-based amphiphilic miktoarm star copolymers having fluoropolymer PVDF and hydrophilic PEO blocks were synthesized *via* a combination of anionic ring-opening, ITP and CuAAC methodologies. The combination of ITP and CuAAC chemistries and the selection of multi-functional precursors allow facile access to different PVDF-based complex macromolecular architectures.

We have shown how chain topology can significantly affect the isothermal crystal phase formation in PVDF. Contrarily to the well-known behavior of linear PVDF materials that crystallize in the α-phase when they are isothermally crystallized from the melt, a linear 2-arm block copolymer (($PVDF_{29}$-N$_3$)$_2$) exhibits a polymorphic behavior (with a predominant β-phase formation) during melting after isothermal crystallization that significantly depends on the temperature of crystallization. Analysis of the multiple melting behavior indicates that the sample forms both α and β-phases, where the α -phase transforms into the γ-phase during isothermal crystallization.

In the case of the more complex $(PVDF)_2(PEO)_2$ 4-miktoarm star block copolymers, we found a remarkable behavior, as the PVDF arms only form the ferroelectric β-phase when all three materials were isothermally crystallized regardless of the crystallization temperature employed. The presence of exclusive β-phase was corroborated by DSC and FTIR. Hence, we have shown that tailoring chain topology in PVDF copolymers can lead to exclusive β-phase formation, a path that can be exploited for future piezoelectric applications.

Author contributions

The manuscript was written with the contributions of all authors. All authors have approved the final version of the manuscript.

Declaration of Competing Interest

The authors declare that they have no known competing financial interests or personal relationships that could have appeared to influence the work reported in this paper.
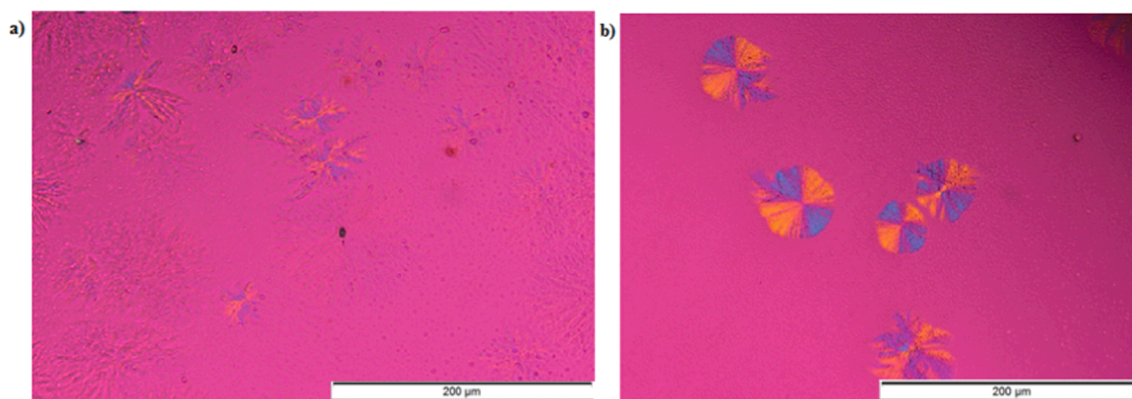
Fig. 11. a) $(PVDF_{66})_2(PEO_{227})_2$ and b) $(PVDF_{106})_2(PEO_{159})_2$ crystals during an isothermal crystallization at 140 °C.

Data availability

Data will be made available on request.

***Data** availability*

The raw/processed data required to reproduce these findings cannot be shared at this time as the data also forms part of an ongoing study. In any case, most of the processed data is reported here and in the SI.

Appendix A. Supplementary material

Supplementary data to this article can be found online at https://doi.org/10.1016/j.eurpolymj.2022.111506.

References

[1] X. Yuan, S. Changgeng, G. Yan, Z. Zhenghong, Application review of dielectric electroactive polymers (DEAPs) and piezoelectric materials for vibration energy harvesting, J. Phys. Conf. Ser. 744 (2016) 012077.

[2] B. Ameduri, B. Boutevin, Well-architectured fluoropolymers: synthesis, properties and applications, Elsevier, 2004.

[3] R.G. Kepler, R.A. Anderson, Ferroelectric polymers, Adv. Phys. 41 (1) (1992) 1–57.

[4] P. Ueberschlag, PVDF piezoelectric polymer, Sensor Rev. 21 (2) (2001) 118–126.

[5] P. Martins, A.C. Lopes, S. Lanceros-Mendez, Electroactive phases of poly (vinylidene fluoride): Determination, processing and applications, Prog. Polym. Sci. 39 (4) (2014) 683–706.

[6] Z.H. Liu, C.T. Pan, L.W. Lin, H.W. Lai, Piezoelectric properties of PVDF/MWCNT nanofiber using near-field electrospinning, Sens. Actuators, A 193 (2013) 13–24.

[7] D. Guyomar, S. Pruvost, G. Sebald, Energy harvesting based on FE-FE transition in ferroelectric single crystals, IEEE Trans. Ultrason. Ferroelectr. Freq. Control 55 (2) (2008) 279–285.

[8] J.B. Lando, W.W. Doll, The polymorphism of poly(vinylidene fluoride). I. The effect of head-to-head structure, J. Macromol. Sci. Part B 2 (2) (1968) 205–218.

[9] A.J. Lovinger, Ferroelectric polymers, Science 220 (4602) (1983) 1115–1121.

[10] P. Eskandari, Z. Abousalman-Rezvani, H. Roghani-Mamaqani, M. Salami-Kalajahi, Polymer-functionalization of carbon nanotube by in situ conventional and controlled radical polymerizations, Adv. Colloid Interface Sci. 294 (2021) 102471.

[11] K. Tashiro, M. Kobayashi, H. Tadokoro, E. Fukada, Calculation of elastic and piezoelectric constants of polymer crystals by a point charge model: application to poly(vinylidene fluoride) Form I, Macromolecules 13 (3) (1980) 691–698.

[12] J.B. Lando, H.G. Olf, A. Peterlin, Nuclear magnetic resonance and x-ray determination of the structure of poly(vinylidene fluoride), J. Polym. Sci. Part A-1 Polym. Chem. 4 (4) (1966) 941–951.

[13] A.J. Lovinger, Crystallization and morphology of melt-solidified poly(vinylidene fluoride), J. Polym. Sci.: Polym. Phys. Ed. 18 (4) (1980) 793–809.

[14] G. Cortili, G. Zerbi, Further infra-red data on polyvinylidene fluoride, Spectrochim. Acta, Part A 23 (7) (1967) 2216–2218.

[15] M. Bachmann, W.L. Gordon, S. Weinhold, J.B. Lando, The crystal structure of phase IV of poly(vinylidene fluoride), J. Appl. Phys. 51 (10) (1980) 5095–5099.

[16] M.A. Bachmann, W.L. Gordon, J.L. Koenig, J.B. Lando, An infrared study of phase-III poly(vinylidene fluoride), J. Appl. Phys. 50 (10) (1979) 6106–6112.

[17] M. Li, H.J. Wondergem, M.-J. Spijkman, K. Asadi, I. Katsouras, P.W.M. Blom, D. M. de Leeuw, Revisiting the δ-phase of poly(vinylidene fluoride) for solution-processed ferroelectric thin films, Nat. Mater. 12 (2013) 433.

[18] A.J. Lovinger, Poly(Vinylidene Fluoride), in: D.C. Bassett (Ed.), Developments in Crystalline Polymers—1, Springer Netherlands, Dordrecht, 1982, pp. 195-273.

[19] V.S.D. Voet, G. ten Brinke, K. Loos, Well-defined copolymers based on poly (vinylidene fluoride): From preparation and phase separation to application, J. Polym. Sci., Part A: Polym. Chem. 52 (20) (2014) 2861–2877.

[20] B. Ameduri, Controlled Radical (Co)polymerization of Fluoromonomers, Macromolecules 43 (24) (2010) 10163–10184.

[21] B. Ameduri, From Vinylidene Fluoride (VDF) to the Applications of VDF-Containing Polymers and Copolymers: Recent Developments and Future Trends, Chem. Rev. 109 (12) (2009) 6632–6686.

[22] M. Guerre, B. Campagne, O. Gimello, K. Parra, B. Ameduri, V. Ladmiral, Deeper Insight into the MADIX Polymerization of Vinylidene Fluoride, Macromolecules 48 (21) (2015) 7810–7822.

[23] G. Lopez, M. Guerre, B. Améduri, J.-P. Habas, V. Ladmiral, Photocrosslinked PVDF-based star polymer coatings: an all-in-one alternative to PVDF/PMMA blends for outdoor applications, Polym. Chem. 8 (20) (2017) 3045–3049.

[24] D.E. Apostolides, C.S. Patrickios, T. Sakai, M. Guerre, G.r. Lopez, B. Améduri, V. Ladmiral, M. Simon, M. Gradzielski, D. Clemens, Near-model amphiphilic polymer conetworks based on four-arm stars of poly (vinylidene fluoride) and poly (ethylene glycol): synthesis and characterization, Macromolecules 51(7) (2018) 2476-2488.

[25] V.S. Voet, G.O.A. van Ekenstein, N.L. Meereboer, A.H. Hofman, G. ten Brinke, K. Loos, Double-crystalline PLLA-b-PVDF-b-PLLA triblock copolymers: preparation and crystallization, Polym. Chem. 5 (7) (2014) 2219–2230.

[26] (a) C. Boyer, D. Valade, L. Sauguet, B. Ameduri, B. Boutevin, Iodine Transfer Polymerization (ITP) of Vinylidene Fluoride (VDF). Influence of the Defect of VDF Chaining on the Control of ITP, Macromolecules 38(25) (2005) 10353-10362, (b) C. Boyer, D. Valade, P. Lacroix-Desmazes, B. Ameduri, B. Boutevin, Kinetics of the iodine transfer polymerization of vinylidene fluoride, Journal of Polymer Science Part A: Polymer Chemistry 44(19) (2006) 5763-5777.

[27] (a) C. Boyer, D. Valade, L. Sauguet, B. Ameduri, B. Boutevin, Iodine Transfer Polymerization (ITP) of Vinylidene Fluoride (VDF). Influence of the Defect of VDF Chaining on the Control of ITP, Macromolecules 38(25) (2005) 10353-10362, (b) C. Boyer, D. Valade, P. Lacroix-Desmazes, B. Ameduri, B. Boutevin, Kinetics of the iodine transfer polymerization of vinylidene fluoride, Journal of Polymer Science Part A: Polymer Chemistry 44(19) (2006) 5763-5777.

[28] S. Junnila, N. Houbenov, S. Hanski, H. Iatrou, A. Hirao, N. Hadjichristidis, O. Ikkala, Hierarchical Smectic Self-Assembly of an ABC Miktoarm Star Terpolymer with a Helical Polypeptide Arm, Macromolecules 43 (21) (2010) 9071–9076.

[29] H. Gao, K. Matyjaszewski, Synthesis of Star Polymers by a Combination of ATRP and the "Click" Coupling Method, Macromolecules 39 (15) (2006) 4960–4965.

[30] S. Bates Frank, Polymer-Polymer Phase Behavior, Science 251 (4996) (1991) 898–905.

[31] F.S. Bates, G.H. Fredrickson, Block copolymers-designer soft materials, Phys. Today 52 (2) (1999) 32–38.

[32] Y. Mai, A. Eisenberg, Self-assembly of block copolymers, Chem. Soc. Rev. 41 (18) (2012) 5969–5985.

[33] T. Kaura, R. Nath, M.M. Perlman, Simultaneous stretching and corona poling of PVDF films, J. Phys. D Appl. Phys. 24 (10) (1991) 1848–1852.

[34] A. Altomare, M. Bozorg, K. Loos, PVDF-based multiferroic, Fascinating Fluoropolymers and Their Applications, Elsevier, 2020, pp. 45-81.

[35] C.M. Costa, V.F. Cardoso, R. Brito-Pereira, P. Martins, D.M. Correia, V. Correia, C. Ribeiro, P.M. Martins, S. Lanceros-Méndez, Chapter 1 - Electroactive poly

(vinylidene fluoride)-based materials: recent progress, challenges, and opportunities, in: B. Ameduri, S. Fomin (Eds.), Fascinating Fluoropolymers and Their Applications, Elsevier, 2020, pp. 1-43.

[36] E. Bihler, K. Holdik, W. Eisenmenger, Polarization distributions in isotropic, stretched or annealed PVDF films, IEEE Trans. Electr. Insul. 24 (3) (1989) 541–545.

[37] S.J. Kang, Y.J. Park, I. Bae, K.J. Kim, H.-C. Kim, S. Bauer, E.L. Thomas, C. Park, Printable Ferroelectric PVDF/PMMA Blend Films with Ultralow Roughness for Low Voltage Non-Volatile Polymer Memory, Adv. Funct. Mater. 19 (17) (2009) 2812–2818.

[38] M. Li, N. Stingelin, J.J. Michels, M.-J. Spijkman, K. Asadi, K. Feldman, P.W. M. Blom, D.M. de Leeuw, Ferroelectric Phase Diagram of PVDF:PMMA, Macromolecules 45 (18) (2012) 7477–7485.

[39] N. María, J. Maiz, D.E. Martínez-Tong, A. Alegria, F. Algarni, G. Zapzas, N. Hadjichristidis, A.J. Müller, Phase Transitions in Poly(vinylidene fluoride)/ Polymethylene-Based Diblock Copolymers and Blends, Polymers 13 (15) (2021) 2442.

[40] N.L. Meereboer, I. Terzić, P. van der Steeg, M. Acuautla, V.S.D. Voet, K. Loos, Electroactive behavior on demand in Poly(vinylidene fluoride-co-vinyl alcohol) copolymers, Mater. Today Energy 11 (2019) 83–88.

[41] K. Tashiro, K. Takano, M. Kobayashi, Y. Chatani, H. Tadokoro, Structure and ferroelectric phase transition of vinylidene fluoride-trifluoroethylene copolymers: 2. VDF 55% copolymer, Polymer 25 (2) (1984) 195–208.

[42] G.T. Davis, M.G. Broadhurst, A.J. Lovinger, T. Furukawa, Hysteresis in copolymers of vinylidene fluoride and trifluoroethylene, Ferroelectrics 57 (1) (1984) 73–84.

[43] C. Li, P. Wu, S. Lee, A. Gorton, M.J. Schulz, C.H. Ahn, Flexible Dome and Bump Shape Piezoelectric Tactile Sensors Using PVDF-TrFE Copolymer, J. Microelectromech. Syst. 17 (2) (2008) 334–341.

[44] T. Soulestin, V. Ladmiral, F.D. Dos Santos, B. Améduri, Vinylidene fluoride- and trifluoroethylene-containing fluorinated electroactive copolymers. How does chemistry impact properties? Prog. Polym. Sci. 72 (2017) 16–60.

[45] N.L. Meereboer, I. Terzić, S. Saidi, D. Hermida Merino, K. Loos, Nanoconfinement-Induced β-Phase Formation Inside Poly(vinylidene fluoride)-Based Block Copolymers, ACS Macro Lett. 7 (7) (2018) 863–867.

[46] M. Zhang, S. Tan, J. Xiong, C. Chen, Y. Zhang, X. Wei, Z. Zhang, Tailoring Dielectric and Energy Storage Performance of PVDF-Based Relaxor Ferroelectrics with Hydrogen Bonds, ACS Applied Energy Materials 4 (8) (2021) 8454–8464.

[47] F. Lederle, C. Härter, S. Beuermann, Inducing β phase crystallinity of PVDF homopolymer, blends and block copolymers by anti-solvent crystallization, J. Fluorine Chem. 234 (2020), 109522.

[48] N. María, J. Maiz, V. Rodionov, N. Hadjichristidis, A.J. Müller, 4-Miktoarm star architecture induces PVDF β-phase formation in (PVDF)2-b-(PEO)2 miktoarm star copolymers, J. Mater. Chem. C 8 (39) (2020) 13786–13797.

[49] E. Pérez, I. Angulo, E. Blázquez-Blázquez, M.L. Cerrada, Characteristics of the Non-Isothermal and Isothermal Crystallization for the β Polymorph in PVDF by Fast Scanning Calorimetry, Polymers 12 (11) (2020).

[50] A. Salimi, A.A. Yousefi, Conformational changes and phase transformation mechanisms in PVDF solution-cast films, J. Polym. Sci., Part B: Polym. Phys. 42 (18) (2004) 3487–3495.

[51] M.P. Silva, V. Sencadas, G. Botelho, A.V. Machado, A.G. Rolo, J.G. Rocha, S. Lanceros-Mendez, α- and γ-PVDF: Crystallization kinetics, microstructural variations and thermal behaviour, Mater. Chem. Phys. 122 (1) (2010) 87–92.

[52] A.T. Lorenzo, M.L. Arnal, J. Albuerne, A.J. Müller, DSC isothermal polymer crystallization kinetics measurements and the use of the Avrami equation to fit the data: Guidelines to avoid common problems, Polym. Test. 26 (2) (2007) 222–231.

[53] V.O. Rodionov, V.V. Fokin, M.G. Finn, Mechanism of the Ligand-Free CuI-Catalyzed Azide-Alkyne Cycloaddition Reaction, Angew. Chem. Int. Ed. 44 (15) (2005) 2210–2215.

[54] J.M. Ren, T.G. McKenzie, Q. Fu, E.H.H. Wong, J. Xu, Z. An, S. Shanmugam, T. P. Davis, C. Boyer, G.G. Qiao, Star Polymers, Chem. Rev. 116 (12) (2016) 6743–6836.

[55] P.C. Hiemenz, T.P. Lodge, Polymer Chemistry, second ed., CRC Press, 2007.

[56] G. Reiter, G.R. Strobl, Progress in Understanding of Polymer Crystallization, Springer, 2007.

[57] M. Avrami, Granulation, phase change, and microstructure kinetics of phase change, III, J. Chem. Phys. 9 (2) (1941) 177–184.

[58] T. Miyazaki, Y. Takeda, M. Akasaka, M. Sakai, A. Hoshiko, Preparation of Isothermally Crystallized γ-Form Poly(vinylidene fluoride) Films by Adding a KBr Powder as a Nucleating Agent, Macromolecules 41 (7) (2008) 2749–2753.

[59] V. Sencadas, C.M. Costa, J.L. Gómez Ribelles, S. Lanceros-Mendez, Isothermal crystallization kinetics of poly(vinylidene fluoride) in the α-phase in the scope of the Avrami equation, J. Mater. Sci. 45 (5) (2010) 1328–1335.

[60] Z. Cui, N.T. Hassankiadeh, Y. Zhuang, E. Drioli, Y.M. Lee, Crystalline polymorphism in poly(vinylidenefluoride) membranes, Prog. Polym. Sci. 51 (2015) 94–126.

[61] J. Martín, D. Zhao, T. Lenz, I. Katsouras, D.M. De Leeuw, N. Stingelin, Solid-state-processing of δ-PVDF, Mater. Horiz. 4 (3) (2017) 408–414.

[62] M.M. Abolhasani, M. Naebe, Q. Guo, A new approach for mechanisms of ferroelectric crystalline phase formation in PVDF nanocomposites, PCCP 16 (22) (2014) 10679–10687.

[63] M.M. Abolhasani, F. Zarejousheghani, Z. Cheng, M. Naebe, A facile method to enhance ferroelectric properties in PVDF nanocomposites, RSC Adv. 5 (29) (2015) 22471–22479.

[64] K. Asai, K. Okamoto, K. Tashiro, Crystallization behavior of nano-composite based on poly(vinylidene fluoride) and organically modified layered titanate, Polymer 49 (19) (2008) 4298–4306.

[65] H. Wang, X. Yang, Y. Zhao, C. Yan, S. Wang, H. Yang, X. Wang, J.M. Schultz, Preparation of gamma-PVDF with controlled orientation and insight into phase transformation, Polymer 123 (2017) 282–289.

[66] R. Gregorio, R.C. CapitāO, Morphology and phase transition of high melt temperature crystallized poly(vinylidene fluoride), J. Mater. Sci. 35 (2) (2000) 299–306.

[67] M. Wang, S. Wang, J. Hu, H. Li, Z. Ren, X. Sun, H. Wang, S. Yan, Taming the Phase Transition Ability of Poly(vinylidene fluoride) from α to γ′ Phase, Macromolecules 53 (14) (2020) 5971–5979.

[68] W.M. Prest, D.J. Luca, The morphology and thermal response of high-temperature–crystallized poly(vinylidene fluoride), J. Appl. Phys. 46 (10) (1975) 4136–4143.

[69] S. Osaki, Y. Ishida, Effects of annealing and isothermal crystallization upon crystalline forms of poly(vinylidene fluoride), J. Polym. Sci.: Polym. Phys. Ed. 13 (6) (1975) 1071–1083.

[70] A.J. Lovinger, Crystalline transformations in spherulites of poly(vinylidene fluoride), Polymer 21 (11) (1980) 1317–1322.

[71] K. Nakagawa, Y. Ishida, Annealing effects in poly(vinylidene fluoride) as revealed by specific volume measurements, differential scanning calorimetry, and electron microscopy, J. Polym. Sci.: Polym. Phys. Ed. 11 (11) (1973) 2153–2171.

[72] T. Yoshihara, H. Tadokoro, S. Murahashi, Normal Vibrations of the Polymer Molecules of Helical Conformation. IV. Polyethylene Oxide and Polyethylene-d4 Oxide, J. Chem. Phys. 41 (9) (1964) 2902–2911.

[73] S. Lanceros-Méndez, J.F. Mano, A.M. Costa, V.H. Schmidt, FTIR and DSC studies of mechanically deformed β-PVDF films, J. Macromol. Sci. Part B 40 (3–4) (2001) 517–527.

[74] T. Boccaccio, A. Bottino, G. Capannelli, P. Piaggio, Characterization of PVDF membranes by vibrational spectroscopy, J. Membr. Sci. 210 (2) (2002) 315–329.